SME Annual Meeting
Mar. 01 - 05, 2021, Denver, CO

Preprint 21-051

ECONOMICAL, LOW-PROFILE CAPACITIVE LOAD CELLS FOR UNDERGROUND MINING TOOL WEAR ESTIMATION AND MATERIAL CLASSIFICATION TO PROMOTE WORKER SAFETY

A. F. Oltmanns, Colorado School of Mines, Golden, CO
A. J. Petruska, Colorado School of Mines, Golden, CO

ABSTRACT

A capacitive load cell made using FlexPCB manufacturing technology, is shown to be a feasible approach for *in-situ* sensing of continuous mining vibration signatures. Capacitive sensors are known for being resilient to temperature variations and the chosen materials are widely available. A batch of example sensors are characterized with load frame testing. Changes in capacitance due to strain from applied force is measured with an embedded capacitance meter. Algorithms which accurately classify vibration signals to determine tool wear and material type are discussed. Considerations for device packaging and integration with commercially available cutting systems are given.

INTRODUCTION

Unforeseen maintenance delays reduce production time [1]. Continuous mining operations are hazardous due to the large machines, the potential for roof fall, and the dark, noisy, and dusty environment. This is further complicated by the need for operators to actively monitor important process information and creates dangerous conditions for the operators [2]. Previous efforts to remove miners from the machine and diagnose continuous miner issues in an automated fashion have focused on the hydraulics of the system [1]. Other efforts aim to reduce mining hazards by instrumenting personnel and monitoring their location near the machine [3]. Here we propose that remote and automated collection of process feedback will alleviate some of these hazards by freeing the operator's attention and allowing them to be at a greater distance from the machine.

Typical predictive maintenance techniques involve estimation of tool wear through the use of force or vibration feedback [4] [5]. Material identification techniques also use metrics based in force and energy measurements [6] [7]. Both predictive maintenance and material identification are vibration classification problems. Vibration classification lends itself towards certain standard signal processing and classification techniques primarily in the frequency domain [8].

In underground coal seam mining, the issue is not processing power or algorithm choice, but instead it is the extreme environment, which makes instrumenting the equipment difficult. Any device used must be able to withstand harsh conditions, be safe to operate in an explosive atmosphere, and be economically viable. Designing a sensor to operate in this environment is a difficult task, but other harsh environment applications have found success with capacitive sensors [9]. Other devices that involve resistive elements are susceptible to the intrinsic relationship between temperature and resistance [10]. Typical load cells rely on resistive elements, but new forms of capacitive pressure sensors are a promising technology for new applications.

For the continuous mining of coal seams, it is desired to instrument each pick on the drum of the miner. Dull cutting tools produce more dust and require more energy to mine a volume than sharp tools [6] [11]. As a result, the picks are replaced regularly. Determining the optimal time to replace each pick can improve mine efficiency, but requires detailed data. In order to achieve *in-situ* pick sensing and wear estimation, we present a design for a force sensor that can be embedded into an individual pick.

The remainder of this article is structured as follows. First, a discussion of the physical constrains, general design, modelling, and manufacture of the proposed sensor is given. Then, the method of empirical characterization is presented. Finally, results are given along with remarks, plans for future work, and conclusions.

SENSOR DESIGN

Due to the low pass filtering of mechanical systems, measurement sensitivity decreases the further the sensor is from the source. However, if the sensor is too close to the mining interface, the device may be damaged. Therefore, it is proposed to place the force sensor slightly behind the pick tip.

This location on the tool has tight space constraints. To fit, the device thickness must be less than 25.4 mm (0.1 in) in order to not interfere with the tool's existing design. Designing for redundant measurements, even in this confined space, can improve data reliablity [12]. A mockup of the proposed sensor design is shown in Fig. 1.

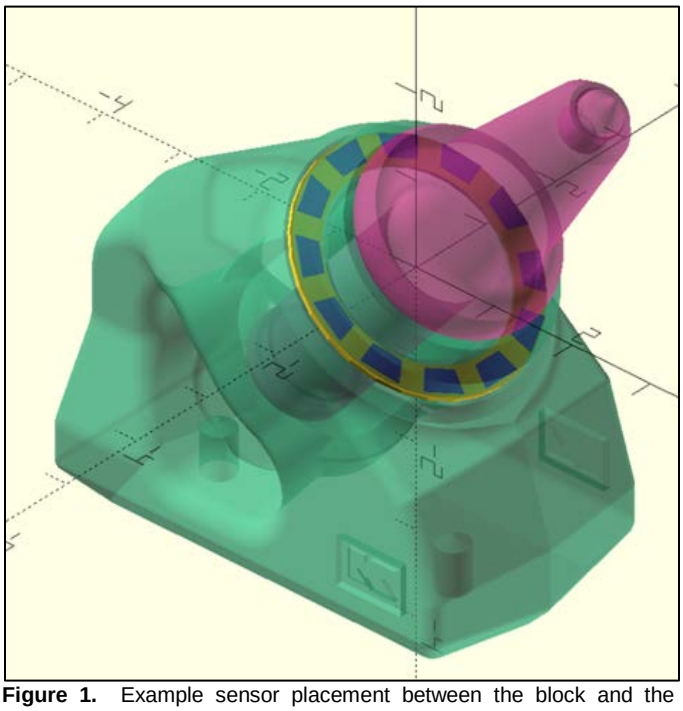

Figure 1. Example sensor placement between the block and the sleeve. The blue trapezoidal sections represent individual sensors. Note that the final sensor geometry is slightly different.

Theory of Operation

In a capacitive load cell, the distance between the plates may be calculated from the capacitance reading by inverting the parallel plate equation:

$$d = \varepsilon_0 \varepsilon_r \frac{A}{C}, \quad (1)$$

where *C* is the sensor's capacitance in Farads, ε_0 is the dielectric permittivity of a vacuum, ε_r is the relative permittivity of the dielectric, *A* is the overlapping area of the plates, and *d* is the distance between them [13]. Note: the capacitance measurement is derived from a resonant frequency measurement of an inductor in parallel with the capacitive sensing element. The resonant frequency, *f* of the resulting circuit is:

$$f = \frac{1}{2\pi\sqrt{LC}}, \tag{2}$$

where *L* is the shunt inductor's value in Henries and *C* is again the sensor's capacitance [14]. It should be noted that the plate distance is proportional to the square of the resonant frequency:

$$d = 4\pi^2\varepsilon_0\varepsilon_r AL f^2 \tag{3}$$

Capacitive sensors are designed such that the plates do not nominally touch given zero applied force, so (3) can be expanded about the nominal separation distance and frequency

$$\Delta d = 4\pi^2\varepsilon_0\varepsilon_r AL(2f_0\Delta f + \Delta f^2) \tag{4}$$

where f_0 is the nominal resonance frequency. The system asymptotes to a linear relationship as the nominal frequency increases, which is also advantages to measurement response time. Assuming f_0 is much larger than the change in frequency Δf resulting from displacement, (4) can be combined with (1) and rewritten as:

$$\Delta f = \frac{1}{4\pi\sqrt{\varepsilon_0\varepsilon_r AL d_0}}\Delta d. \tag{5}$$

where $d_0$is the nominal plate separation distance. It can be seen from Eq. (5) the measurement sensitivity will decrease with increasing plate area, separation distance, inductance, or dielectric permittivity. However, note that (1) neglects fringing field effects, so it is necessary to have a relatively large plate area with a smaller separation distance for the underlying capacitance model.

Since the system will be in a dynamic environment, the vibratinoal modes of the sensor must be considered as well. Dynamically, we model the proposed sensor in two sections: the mass resting on the sensor and the internals of the sensor. This is shown in Fig. 2 The internals of the sensor, modeled as two masses and three springs, have two modes of vibration. The mass resting on the sensor has just one mode of vibration. The inner system (and to a lesser effect, the outer system) is subject If the outer system of the mass on the sensor has a much lower resonant frequency than the resonant frequencies of the internal sensing element, then the lower resonant frequency of the outer system will dominate, and the higher frequency modes of the internal sensing element may be neglected.

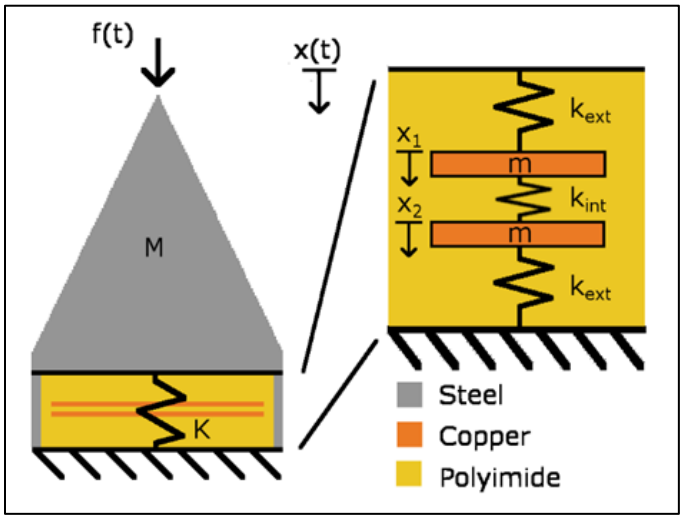

Figure 2. Sensor system dynamic model representation. The system can be considered as two cascaded mass spring systems. The outer system is a relatively large mass resting on a steel housing which contains the sensor internals. It has a lower frequency dominant mode than the inner system. The inner system holds two copper plates suspended in polyimide. It is possible to excite the in-phase and anti-phase modes of this system, but they resonate at much higher frequencies than the dominant mode of the outer system.

Not pictured in Fig. 2 are the damping elements which capture some of the viscoplastic behaviours of the polyimide. [15]. With the given model, the dynamics equations describing the motion of the system due to input force are as follows:

$$M\ddot{x} + Kx = f(t) \tag{6}$$

$$\begin{bmatrix} m & 0 \\ 0 & m \end{bmatrix}\begin{bmatrix} \ddot{x}_1 \\ \ddot{x}_2 \end{bmatrix} + \begin{bmatrix} c & 0 \\ 0 & c \end{bmatrix}\begin{bmatrix} \dot{x}_1 \\ \dot{x}_2 \end{bmatrix} + \begin{bmatrix} k_{ext}+k_{int} & -k_{int} \\ -k_{int} & k_{ext}+k_{int} \end{bmatrix}\begin{bmatrix} x_1 \\ x_2 \end{bmatrix} = \begin{bmatrix} (x-x_1)k_{ext} \\ 0 \end{bmatrix} \tag{7}$$

where *M* is the combined mass of the pick and sleeve, *K* is the overall stiffness of the sensor, *x* is the position of the top plate of the sensor, $\ddot{x}$ is its acceleration, *f(t),* is the applied force at the pick tip, *m* is the equivalent mass one of the internal plates suspended in the dielectric, k_{ext} and k_{int} are the equivalent spring constants for the regions on the exterior and interior of the plates respectively, *c* is the damping coefficient for the substrate, and x_1 and x_2 are the displacements of the plates, which are nominally both zero. Then we may relate the dynamic model to the capacitive model by:

$$\Delta d = x_2 - x_1 \tag{8}$$

The primary mass of the system, *M* may be calculated by the product of the density and volume of the supported portion of the tool. The smaller masses ,*m,* may be calculated as effective masses which combine the effects of the mass of the polyimide and its elasticity by using the common massive spring simplification where the mass is moved to the end of the spring and given an effective value of one third the total mass. The spring constants, *K,* k_{ext}, and k_{int} may be calculated with the standard formula:

$$k = EA/L \tag{9}$$

where E, A, L are the Young's modulus, cross sectional area, and length of the appropriate sections. The damping coefficient, *c,* is given by [15] as:

$$c = 20679.8\, A/L \tag{10}$$

where *A* is the cross sectional area and *L* is the length of the substrate.

Load Cell Design

The measurements taken with the sensor must contain enough information to be used in either analytical models like [17] [18] [19] or data-driven models such as [20] [21] [22]. With the simple model presented above, a minimum of four cells is required for the prototype to provide three axial force measurements with respect to the cutting tool's normal, drag, and tangential directions. The sensor has not been designed to detect torsional loads, as these are uncommon for the physical configuration. Initial characterization of the device, focuses on the applied normal force only. It is desired that this sensor is able to measure applied forces well enough to track the average energy in the dominant vibrational modes of the tool for later classification.

By design, the block, sleeve, and pick system is mechanically very stiff and applied forces do not induce significant strain. It is desirable that the sensor does not induce strain beyond what is necessary to make the required measurements. The sensor should also have its own vibrational modes much higher than the cutting system to avoid dynamic interference. To design a sensor with the desired sampling rate, sensitivity and compatible dynamics, it is expedient to first choose a capacitance and resonant frequency which will provide the desired sampling rate and sensitivity within the physical parameters that will produce acceptable dynamics.

Given the constraints on area, plate distance, dielectric constant, and measurement rate, a sensor capacitance in the hundreds of picofarad range yields a cell with good sensitivity and robustness towards the environment. When coupled with the appropriate value inductor, the resonant frequency of the sensing circuit is in a narrow band between 1 and 3 MHz. This is measured with an embedded capacitance meter, Texas Instruments' FDC2114, which records at

13.3 ksps with 7 effective bits for a single channel. With 4 channels simultaneously monitoring, the effective rate is reduced to 3.3 ksps for each channel with the same accuracy.

Steel and FlexPCB (made of polyimide and copper) are well suited to this application because steel is compatible with the mining environment and the FlexPCB is easily manufactured as a capacitive sensor. Typical forces on the pick during cutting operations range from dozens to hundreds of kN applied at the tip in the normal and drag directions [6]. Quoted values for polyimide Young's Modulus and elastic range are 4.0GPa and about 5% respectively [21]. The viscoelastic nature of the polyimide means that the apparent stiffness of the material depends on the loading profile but will generally be softer for quasi-static loadings and stiffer for rapid loadings [22]. Encasing the polyimide device in a steel housing will increase the overall device stiffness, reduce the induced strain, and protect the sensor from wear. By choosing the proper ratio of steel and polyimide cross sectional area, the expected strain range can be controlled.

For the chosen device height of 1.83 mm (0.72 in), and given the nominal 5% elastic strain range of polyimide, the max displacement in the linear range of the overall device is 91 µm. Considering the force range of the available test equipment, a device stiffness of 250 MN/m is targeted which means the device should be mostly linear up to roughly 20 kN of load. This can be adjusted by varying the case walls' thickness. For the chosen sensor geometries, the nominal frequency measurements are is expected to be 1.60 MHz for the large cells and 1.85 MHz for the small cells. Given the embedded capacitance meter's sensitivity and accuracy at these points, a sensitivity of 33.26 kHz/µm and 37.1 kHz/µm is expected for the large and small cells respectively. At the highest gain setting (16x), the embedded capacitance meter has a resolution of 1.63 counts per kHz which translates to 60.4 counts per µm.

The combined mass of a typical sample sleeve and new pick is about 4 Kg. This means that the first order system will have the dominant resonance near 1260 Hz for the chosen overall device stiffness. For the two copper plate masses contained in the polyimide flex circuit, if the masses and compressive elements of the system are allocated as described in Table 1, then the in phase mode will have resonant frequency of about 4.81 MHz and the anti-phase mode will have resonant frequency of about 20.5 MHz. These modes are significantly faster than the measurement frequency but will be very damped by the mechanical system. The inertia of the pick system before the sensing element and the damping present in the polyimide is large enough to effectively low pass filter these frequencies and reduce the potential for aliasing.

Table 1. Parameters for the internal sensor model.

Parameter	Value
m	56 µg
k_{ext}	51.1 GN/m
k_{int}	440 GN/m

After the specifications were developed for the device's dimensions, the internal element and steel case were manufactured. A completed internal element and several assembled prototypes are shown in Fig. 3. To ensure polyimide filled the steel housing, several polyimide shims are laser cut and stacked evenly on the top and bottom of the sensing element, sufficient to fill the 0.46 mm channel, before being sandwiched in the case.

Finally, the FlexPCB is manufactured with alternating layers of Copper and polyimide and minimal adhesive. This results in a consistent plate distance of 25 µm over a large area which provides reliable capacitance measurements. The steel case is manufactured via chemical etching to achieve consistent dimensions economically.

METHODS

A sample device was characterized through sinusoidal load frame testing across 5 frequencies (0.5 Hz, 1 Hz, 2 Hz, 5 Hz, and 10 Hz) and 3 load ranges (0-50kN, 0-100kN, 0-200kN) performed with a Material Test Systems load frame (model: 312.41). For each test frequency and load range, 50 cycles were applied to the device two separate times. The sample was allowed to rest for a few seconds between tests.

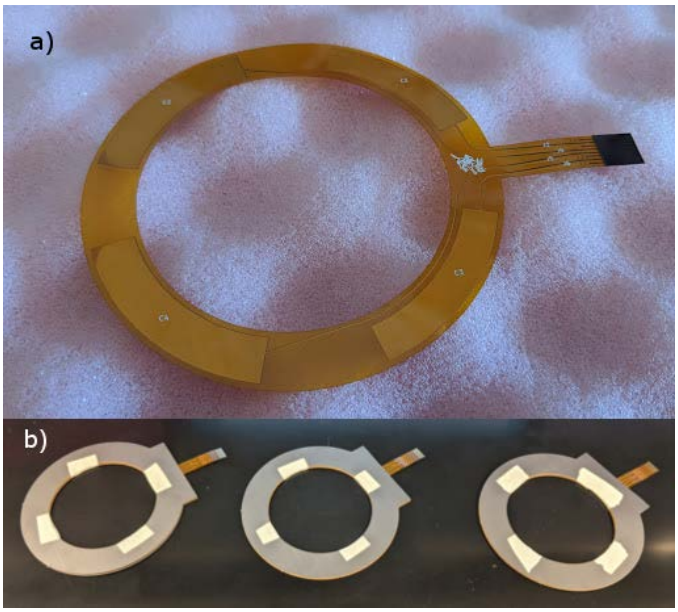

Figure 3. a) A prototype of the sensor internals. The four cells can be seen along with the connector for interfacing with the embedded capacitance meter. As a mitigation for channel crosstalk noise within the load cell, the cells further from the plug are larger and therefore have their resonant frequency a few hundred kHz away from the nearer, smaller cells. b) A few prototype sensors in their cases. The case increases the overall stiffness of the sensor but keeps it less stiff than the surrounding tool.

The device's capacitance is measured using an embedded capacitance sensor interfacing with a data logger (Raspberry Pi 2 Model B v1.1). The load frame tracked the prescribed force loading profiles and measured the resulting force applied and the strain induced on the system. For the low loading rates, a sampling rate of 1024 Hz was used by the load frame and 1450 Hz was used for the capacitive sensor. This is well above the max 10Hz loading of the load cell and will capture any transient effects.

To filter measurement noise in displacement and frequency, a moving average filter (50 samples) and a first order low pass filter (920 Hz -3dB cutoff) are used.. The derivative of frequency was estimated by passing the consecutive differences of the filtered frequency divided by the sampling time through a moving average with the same window size as before. It is used to create a surjective map between measurements and the desired quantities. Through this filtering, it is possilbe to see a clear seperation in the hysteresis plots of the higher rate and higher force loads.

RESULTS

Over large strain ranges, the device exhibited hysteresis in the force-displacement curve due to the viscoelastic nature of the polyimide. For low loading rates, the hysteresis was reduced but still present. A representative plot for the measured data is shown in Fig. 4. The hysteresis plots are also shown in that same figure. It can be seen that viewing force and displacement as functions of measured resonant frequency and its derivative provide a surjective mapping from measurements to the desired quantities. Also, the displacement varies with the measured frequency as predicted by the dynamic model.

DISCUSSION

This embedded system has a relatively small footprint and power demand and would be readily transferable for use in an underground mining environment. The minimal post-processing of data could also

be converted to a real-time process for classification tasks without significantly altering the design.

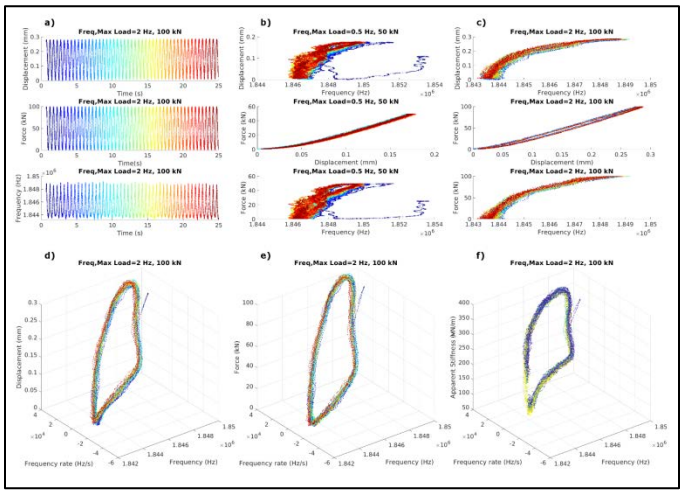

Figure 4. a) A representative loading cycle. The color in the plot represents the passage of time and the corresponding points in the hysteresis graphs are the same color. b) Hysteresis plots for the low rate-low load condition. The relationships are mostly linear but drift while the device settles into a steady state response. c) The hysteresis plots for greater loading. There is more hysteresis and this trend continues for even greater loading. d) The plot of displacement vs measured frequency and its derivative. Note that for each region in the XY plane, there is at most one region that contains the displacement. e) The plot of force vs measured frequency and its derivative. Again, the force is uniquely defined for the presented values of frequency and its derivative. f) The apparent stiffness as a function of measured frequency and its derivative. Again, a surjection is present.

In a simplified physical model, for low load rate condittions and small displacement, the distance between the plates is linear with respect to the overall strain in the sensor and therefore proportional to the square of the resonant frequency. By characterizing the rate-dependent stiffness of the sensing element (due to the viscoelastic polyimide), larger strain rates can be accommodated, and an estimate of applied force can be derived by combining the estimated strain and estimated stiffness of the element.

To integrate this device with continous mining machines, further characterization must be done. It is planned to further characterize this device through experiments on Colorado School of Mine's linear cutting machine which is able to experimentally simulate a single pick cutting through a rock sample. The collected load cell data will be used to develop a classification scheme of tool wear levels and material type.

CONCLUSION

This work shows the preliminary design, construction and characterization of a low-profile load cell for undergond mining applicaoins. Further work is needed in determining processing strategies for the collected data, but it has been shown that a reasonable mapping exists between the desired displacement and applied force quantities and the measured resonant frequency and its derivative. With adequate sampling rates and measurement sensitivity, this device will be able to measure vibration signatures which may be classified into tool wear and material categories.

ACKNOWLEDGEMENT

Funding for this work has been provided by NIOSH contract 75D30119C05413. The opinions expressed here reflect those of the authors and not necessarily NIOSH.

REFERENCES

[1] J. Mitchell, "Research into a sensor-based diagnostic maintenance expert system for the hydraulics of a continuous mining machine," in *Conference Record of the 1991 IEEE Industry Applications Society Annual Meeting*, Dearborn, MI, 1991.

[2] C. Jobes, J. Carr and J. Ducarme, "Evaluation of an Advanced Proximity Detection System for Continuous Mining Machines," *International Journal of Applied Engineering Research,* vol. 7, no. 6, pp. 649-671, 2012.

[3] P. T. Bissert and et al., "Proximity Detection Zones: Designs to Prevent Fatalities Around Continous Mining Machines," *Professional safety,* vol. 61, no. 6, pp. 72-77, 2016.

[4] M. Klaic, Z. Murat, T. Staroveski and D. Brezak, "Tool wear monitoring in rock drilling applications using vibration signals," *Wear,* Vols. 408-409, pp. 222-227, 2018.

[5] I. Abu-Mahfouz, "Drilling wear detection and clasification using vibration signals and artificial neural network," *Machine Tools & Manufacture,* vol. 43, pp. 707-720, 2003.

[6] R. Teale, "The concept of specific energy in rock drilling," *International Journal of Rock Mech. Mining Science,* vol. 2, pp. 57-73, 1965.

[7] N. Klyuchnikov and et al., "Data-driven model for the identification of the rock type at a drilling bit," *Journal of Petroleum Science and Engineering,* vol. 178, pp. 506-516, 2019.

[8] L. Liu, F. Wu, C. Qi, T. Liu and J. Tian, "High frequency vibration analysis in drilling of GFRP laminates using candlestick drills," *Composite Structures,* vol. 184, pp. 742-758, 2018.

[9] L. Chen and M. Mehregany, "A Silicon Carbide Capacitive Pressure Sensor for High Temperature and Harsh Environment Applications," in *TRANSDUCERS 2007 - 2007 International Solid-State Sensors, Actuators and Microsystems Conference*, Lyon, 2007.

[10] D. De Bruyker, A. Cozma and R. Puers, "A Combined Piezoresistive / Capacitive Pressure Sensor With Self-Test Function Based On Thermal Actuation," in *Transducers '97*, Chicago, 1997.

[11] F. F. Roxborough and H. R. Phillips, "Rock excavation by disc cutter," *International Journal of Rock Mechanics and Mining Sciences & Geomechanics Abstracts,* vol. 12, no. 12, pp. 361-366, 1975.

[12] B. Meng, W. Tang, X. Peng and H. Zhang, "Silicon carbide capacitive pressure sensors with arrayed sensing membranes," in *The 8th Annual IEEE International Conference on Nano/Micro Engineered and Molecular Systems*, Suzhou, 2013.

[13] H. Shao, W. Li, D. Dai, B. Liang and F. Lin, "The development of 5 nF parallel-plate capacitors with low voltage coefficient," in *29th Conference on Precision Electromagnetic Measurements (CPEM 2014)*, Rio de Janeiro, 2014.

[14] J. W. Nilsson and S. A. Riedel, "Introduction to the natural response of a parallel RLC circuit," in *Electric Circuits*, Upper Saddle River, Pearson, 2015, p. 269.

[15] B. Y. Dharmadasa, M. McCallum and F. L. Jimenez, "Characterizing and modeling the viscoplastic behaviour of creases in Kapton polyimide films," in *AIAA Scitech 2020 Forum*, Orlando, 2020.

[16] Y. Deng, M. Chen, Y. Jin, Y. Zhang, D. Zou and Y. Lu, "Theoretical and experimental study on the penetration rate for roller cone bits based on the rock dynamic strength and drilling parameters," *Journal of Natural Gas Science and Engineering,* vol. 36, pp. 117-123, 2016.

[17] S. Kalantari, A. Baghbanan and H. Hashemalhosseini, "An analytical model for estimating rock strength parameters from small scale drilling data," *Journal of Rock Mechanics and Geotechnical Engineering,* vol. 11, pp. 135-145, 2019.

[18] Z. Li and K.-i. Itakura, "An analytical drilling model of drag bits for evaluation of rock strength," *Soils and Foundations,* vol. 52, no. 2, pp. 216-227, 2012.

[19] P. Flegner, J. Kačur, M. Durdán and M. Laciak, "Processing a measured vibroacoustic signal for rock type recognition in rotary drilling technology," *Measurement,* vol. 134, pp. 451-467, 2019.

[20] M. He, Z. Zhang, J. Ren, J. Huan, G. Li, Y. Chen and N. Li, "Deep convolutional neural network for fast determination of the rock strength parameters using drilling data," *International Journal of Rock Mechanics and Mining Schiences,* vol. 123, p. 104084, 2019.

[21] C. Hegde and K. E. Gray, "Use of machine learning and data analytics to increase drilling efficiency for nearby wells," *Journal of Natural Gas Science and Engineering,* vol. 40, pp. 327-335, 2017.

[22] W. He and et al., "Study on Young's modulus of thin films on Kapton by microtensile testing combined with dual DIC system," *Surface & Coatings Technology,* vol. 308, pp. 273-279, 2016.

[23] P. J. Wei, W. X. Shen and J. F. Lin, "Analysis and modeling for time-dependent behavior of polymers exhibited in nanoindentation tests," *Journal of Non-Crystalline Solids,* vol. 324, pp. 3911-3918, 2008.